Experimental and numerical study on the initial tip structure evolution of diesel fuel spray under various injection and ambient pressures

Longfei Chen [a], Guangze Li [a], Dongqi Huang [a], Zhichao Zhang [b,c,*], Yiji Lu [b,c,*], Xiaoli Yu [b,c], Anthony Paul Roskilly [b,c]

[a] *School of Energy and Power Engineering, Beihang University, Beijing 100191, China*

[b] *Department of Energy Engineering, Zhejiang University, Hangzhou, 310027, China*

[c] *Sir Joseph Swan Centre for Energy Research, Newcastle University, Newcastle NE1 7RU, UK*

H I G H L I G H T S

- Long-distance microscopy and nanosecond-pulse illumination were adopted.
- Initial spray morphologies at various injection and ambient pressures were studied.
- Four types of spray tip structure were identified and analysed.
- A small liquid column in the 'mushroom' tip was observed and numerically analysed.

Abstract

The formation and evolution of the initial spray structure of diesel fuel in the near-nozzle region under different injection and ambient pressures were studied. A visualisation experiment study on diesel fuel using long-distance microscopy and nanosecond-pulse flashlight was performed. Four types of spray tip structure were identified and named as 'needle', 'bubble', 'mushroom' and 'umbrella'. The obtained high-resolution images revealed that both injection pressure and ambient pressure had a significant influence on the evolution of the spray tip structure. The measurement of the spray penetration and spray angle showed that the increase of injection pressure enhanced spray dispersion while the increase of

E-mail address: zczhang1988@live.com; z.zhang34@ncl.ac.uk (Z. Zhang)
luyiji0620@gmail.com; (Y. Lu)

ambient pressure exhibited an opposite effect. In order to provide a better understanding on the formation mechanism, a numerical study based on large eddy simulation (LES) and volume of fluid (VOF) interface capturing technique was conducted.

Keywords: Initial breakup; Visualisation experiment; Injection pressure; Ambient pressure; Mushroom-shaped structure

1. Introduction

The liquid spray are ubiquitous in the industrial and energy fields such as the application in aviation engines, internal combustion engines [1-3] and cooling towers [4]. Highly dispersed spray has been proven to be extremely important for the engine combustion performance and emissions [5-7]. Fundamental experiments and numerical simulations focused on the initial breakup of liquid spray are essential and significant for improving the operating efficiency of engines because the initial spray behaviours dominate the spray microscopic and macroscopic characteristics [8-10]. The entire liquid injection event can be divided into at least three stages including initial valve opening stage, main injection stage and injection closure stage [11, 12]. Among these three stages, the initial injection is the critical period for the breakup and morphology evolution of liquid jet. Therefore, it is desirable to examine the flow characteristics of the liquid jet in the initial stage, which could provide a useful insight to understand the subsequent combustion processes (droplet dispersion, atomization, evaporation and combustion) [13, 14].

Reported experimental studies mainly focused on the primary breakup of the liquid jet in the opening period. Hattori *et al.* [15] observed the initial breakup process of diesel liquid jet in a high-pressure vessel by employing two different types of illuminations. The aim of this study was mainly focusing on examining the influence of the shearing resistance by the high-pressure ambience on the breakup of liquid fuel to droplets [15]. Wang *et al.* [16] experimentally explored the formation of the mushroom-like head of diesel spray under atmospheric conditions by using a long-distance microscope and an ultra-high-speed camera. The results showed the internal flow regime might be the main factor that influenced the tip

structure of the spray. Fu *et al.* [17] experimentally studied the spray macro characteristics of the mixture of bio-diesel and di-n-butyl ether including spray tip penetration, spray cone angle, maximum spray width and spray tip velocity using a schlieren optical system under different ambient and injection pressures. However, the evolution of tip structure of spray under the same conditions were not reported in their work. Xu *et al.* [18] studied the effects of fuel viscosity and injection pressure on the initial spray patterns in the near-nozzle field for four different fuels including winter diesel, diesel, ethanol and rape methyl ester, and they found that the length of the mushroom was closely related to fuel viscosity. Crua *et al.* [19] captured the high-resolution images of diesel and kerosene spray in the very outset of the injector tip under both atmospheric and realistic engine conditions. It was found that the residual fuel trapped in the nozzle orifice induced an internal vortex motion which could lead to a slipstream effect pushing a liquid column ahead of the liquid jet. Desantes *et al.* [20] investigated the relationship between the in-nozzle cavitation and spray behaviours in the near-nozzle field using visualisation experiments. The results revealed that the existence of the cavitation bubbles in the nozzle exit caused an obvious increment of the spray angle. In summary, previous experimental studies had not yet systematically focused on the initial tip structure evolution of spray under different ambient and injection pressures.

Apart from the experimental studies on the liquid jet structure in the initial stage of spray formation, related numerical studies have also been performed by many researchers. Shinjo and Umemura [21] studied the droplet formation and ligament dynamics in spray tip using direct numerical simulation. The results showed that mushroom-like tip was induced by the impingement of liquid against the still air, and the ligament formation in the periphery of

spray head was triggered by the rolling up effects of the liquid jet tip. The morphology evolution of diesel spray in the early injection stage was numerically and experimentally analysed by Ghiji *et al.* [22] using the volume of fluid (VOF) phase-fraction interface capturing technique. The mushroom-shaped spray head structure was captured in both experiment and simulation. Xiao *et al.* [23] developed a two-phase flow model with large eddy simulation (LES) algorithm to investigate the effects of the in-nozzle liquid flow regimes and gas turbulence on the initial structure of water spray in the co-axial gas flow. It was demonstrated that the in-nozzle liquid regimes and gas turbulence had a critical role in the surface instability of liquid jet. Sun *et al.* [8] predicted the breakup of co-flow liquid jet using a newly developed CFD model, and they revealed that the entrainment effect and intense central-region atomization cause small droplets to concentrate on the spray axis and large droplets to dominate in the peripheral region of the spray. Battistoni *et al.* [24] proposed an Eulerian mixture model using the LES method to study the spray behaviours at the starting and ending stages of injection, they found the residual gas trapped inside the injector sac had a significant influence on fuel injection rate and spray penetration.

In summary, previous researches mainly studied certain mechanisms about the initial spray breakup. However, few of them systematically studied the spray tip structure in the initial injection stage. Moreover, numerical researches on the formation of the liquid column observed in the spray tip were also hardly reported and studied. Therefore, this study has been conducted employing a combined long-distance microscopy and nanosecond-pulse illumination to investigate the breakup of diesel jet at the initial injection stage under three injection pressures (30 MPa, 40 MPa and 50 MPa) and four ambient pressures (0.1 MPa, 0.5

MPa, 1 MPa and 2 MPa). Meanwhile, a numerical study based on LES theory and VOF interface capturing method was attempted for the first time to explore the formation mechanism of a liquid column observed in the tip of the liquid jet.

2. Experimental apparatus and methodology

An electromagnetic injector (Fig. 1) with the orifice diameter of 0.3 mm was adopted, and the length and the inclination angle of the injector orifice were 2 mm and 60°, respectively. The nozzle inclination angle was defined as the angle between the injector and the central axis of the nozzle orifice. The tested fuel was diesel fuel, and its physical properties were stated in Table. 1 along with the experimental conditions. It is worth mentioning that the nozzle was made of perspex for a better observation on the inner activity of the nozzle. Therefore, the maximum injection pressure must less than 60 MPa to avoid the rupture of the perspex nozzle.

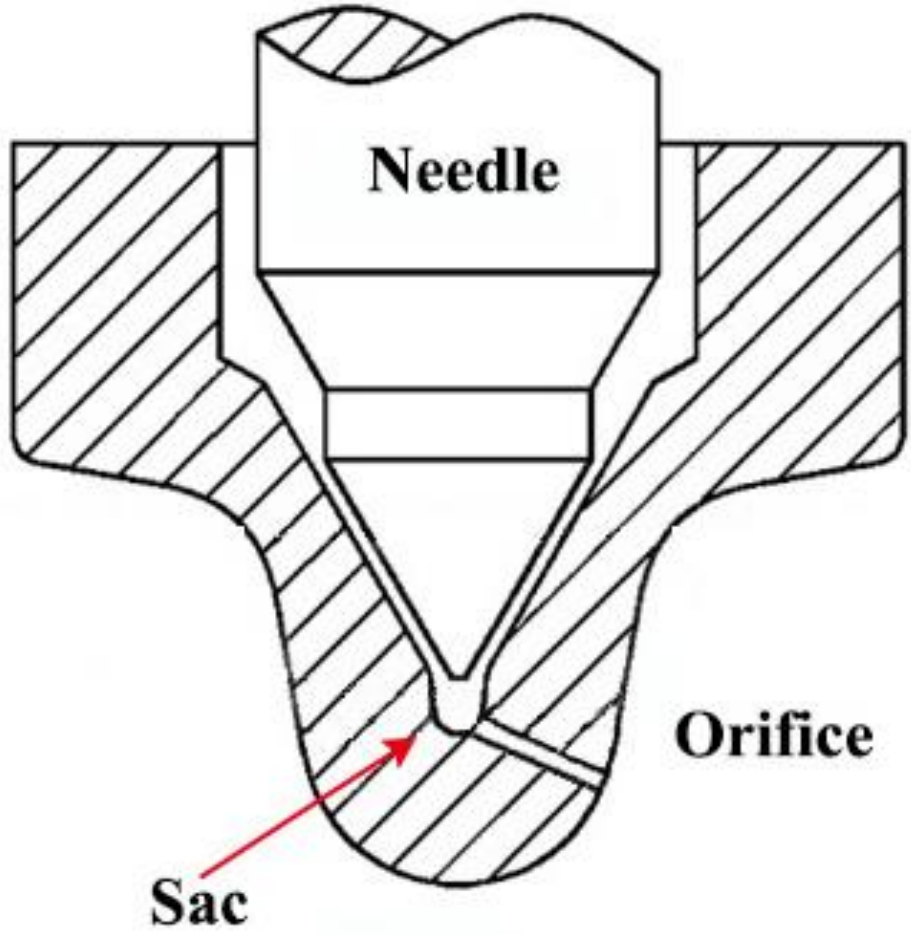

Fig. 1 The schematic diagram of the injector.

Table 1. The diesel fuel properties and experimental conditions

Parameters	Values
Temperature T /K	293
Fuel density $\rho_l/(kg\cdot m^{-3})$	840
Kinematic viscosity $\mu/(m^2\cdot s^{-1})$	$3.049x10^{-6}$
Saturation vapour pressure P_v/Pa	892
Surface tension $\sigma/(N\cdot m^{-1})$	0.002
Air density $\rho_g/(kg\cdot m^{-3})$	1.205
Injection pressures P_i/(MPa)	30, 40, 50

Ambient pressures	P_a/(MPa)	0.1, 0.5, 1, 2

The experimental apparatus mainly consists of five parts as shown in Fig. 2: a fuel supply system, a common rail system, a constant volume chamber, an electronic controlling unit (ECU) and an image acquisition system. The diesel fuel was supplied into the common rail after passing an Inlet Metering Valve (DELPHI IMV 9109-927), then injected through the nozzle in the constant volume chamber. The IMV was used to measure the average mass flow rate for the adopted injector during the injection pulsation of 1 ms, and then the temporal variation of the fuel mass flow rate could be obtained based on the calculation of the average flow velocity within 1 ms. The fuel injection amount was set as 10 mg each time. The pressure of the chamber was regulated by a high-pressure air tank. Two Perspex windows with the size of 122 (length) × 88 (width) × 30 (thickness) millimetres were amounted in both sides of the chamber for the convenience of lighting and shooting. In order to capture the liquid jet breakup process in the near region, a Canon camera (EOS 700D) together with a long-distance microscope (QUESTAR Inc., QM-100) and a nanosecond-pulse flashlight (SUGAWARA Laboratories Inc., NPL-5) were used. The operating distance of the microscope was in the range of 10 to 40 cm, and the microscope resolution is 1.1 μm. The magnification of the microscope was set as 40 (the maximum magnification is 180), and the exposure time of the camera was 180 ns.

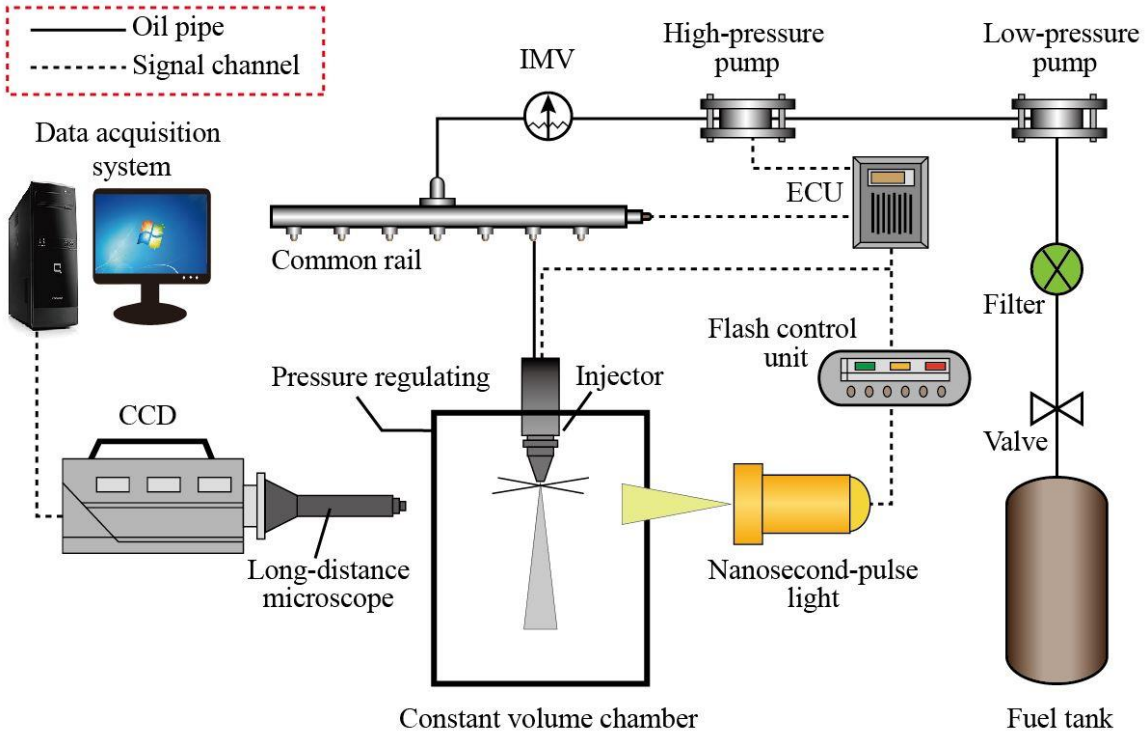

Fig. 2 The schematic diagram of the test rig

The ECU was employed to synchronise the injection signal and flashlight trigger signal. The camera was set at operating mode before an injection event started, then a delay time Δt_1 was designated to the ECU. When the fuel injection signal was received by the ECU, it was transmitted to trigger the flash lamp with the delay time Δt_1, then the camera captured an injection image. A delay time Δt_2 ($\Delta t_1 < \Delta t_2$) would be designated for the next injection imaging. The whole injection process could be recorded by setting different delay times. It is worth noting that the obtained images came from different injections, thus 20 images were acquired at each delay time to reduce the cycle-to-cycle variations. The cycle-to-cycle variation of the images was about 8% (the maximum or minimum value of spray penetration or angle/ average value < 8%), and it was mainly caused by the occasional existence of the mushroom-shaped spray head as reported in Ref. [16].

The obtained images were processed using an in-house program written by MATLAB. The detailed processing procedures were as follows: 1. cropped the original image into a proper size; 2. enhanced the contrast of the image; 3. subtracted the image background; 4. binarised the image with an appropriate threshold. The spray characteristics at the near region were demonstrated in Fig. 3. The penetration lengths were calculated by the number of pixels between the outlet of the injector and the spray tip. The spray angle was defined as the angle between the two spray boundaries as shown in Fig.3.

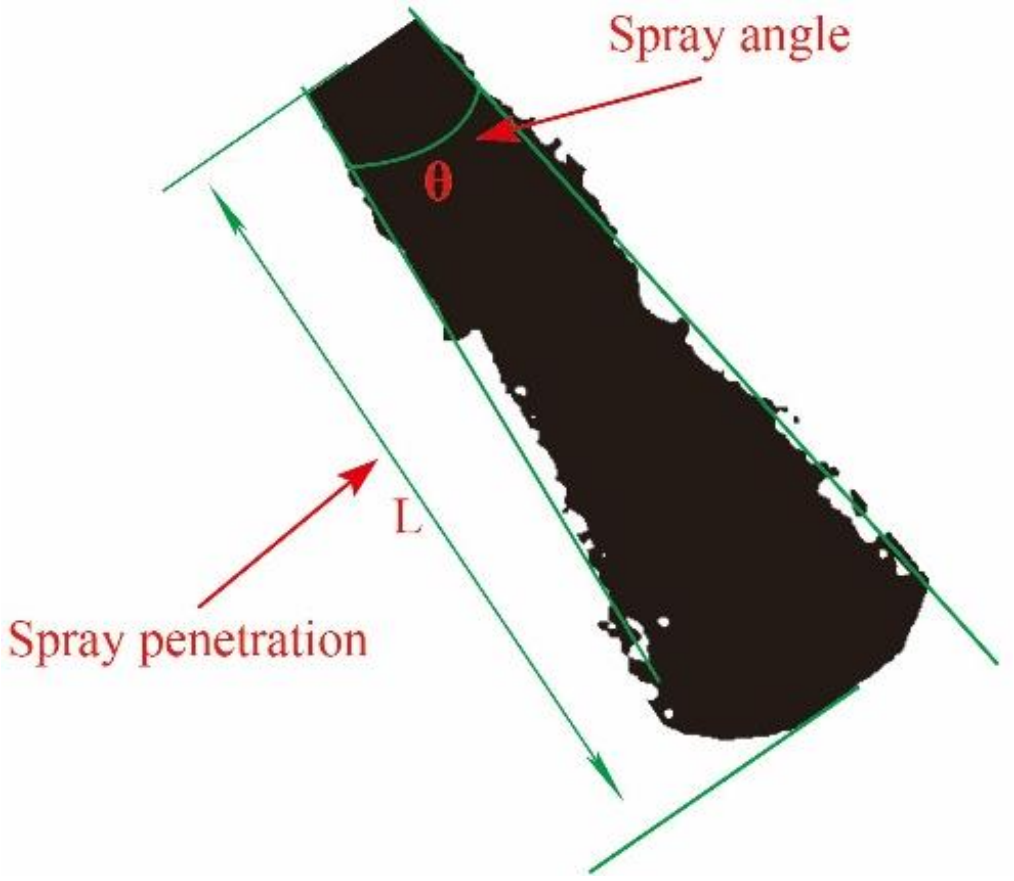

Fig. 3 The measurement of spray characteristic parameters

The formation process of the liquid column observed in the tip of the jet was simulated by employing LES method and VOF interface capturing technique with OpenFOAM. A two-phase homogenous mixture model along with the Schnerr and Sauer cavitation model

[25] was adopted in the simulation.

For two-phase flow, the governing continuity and momentum equations are given by

$$\frac{\partial \rho}{\partial t} + \frac{\partial \rho \bar{u}_i}{\partial x_i} = 0 \tag{1}$$

$$\frac{\partial \bar{u}_i}{\partial t} + \frac{\partial (\bar{u}_i \bar{u}_j)}{\partial x_i} = -\frac{1}{\rho}\frac{\partial \bar{\rho}}{\partial x_i} + \frac{\mu}{\rho}\frac{\partial^2 \bar{u}_i}{\partial {x_j}^2} - \frac{\partial \tau_{ij}}{\partial x_j} \tag{2}$$

Where ρ and μ are the density and viscosity of the mixed-phase, respectively. $\bar{u}$ is filter velocity with the subscript '*i*' and '*j*' representing coordinate. τ_{ij} is the sub-grid stress and can be calculated by Eq. (3) and Eq. (4) [26, 27]:

$$\tau_{ij} = 1/3(\tau_{kk}\delta_{ij}) - 2v_t\bar{s}_{ij} \tag{3}$$

$$\bar{s}_{ij} = 1/2(\frac{\partial \bar{u}_i}{\partial x_j} + \frac{\partial \bar{u}_j}{\partial x_i}) \tag{4}$$

Where $\bar{s}_{ij}$ is the deformation rate tensor in large scale, and δ_{ij} is the Kronecker parameter. v_t is the Sub-grid turbulent viscosity which is given by [28]:

$$v_t = C_k \Delta \sqrt{k_t} \tag{5}$$

Where C_k is constant and equal to 0.094, Δ is the mesh size. k_t represents the turbulent kinetic energy in the sub-grid scale, thus the sub-grid turbulent kinetic energy transport equation is

$$\frac{\partial k_t}{\partial t} + \frac{\partial \bar{u}_j k_t}{\partial x_j} = -\tau_{ij}\left(\frac{\partial \bar{u}_i}{\partial x_j}\right) - C_\epsilon \frac{k_t^{3/2}}{\Delta} + \frac{\partial (\frac{\partial k_t}{\partial x_j}\frac{v_t}{\sigma_k})}{\partial x_i} \tag{6}$$

Where C_ϵ and σ_k are constant and equal to 1.048 and 1 independently.

The Schnerr and Sauer cavitation model was based on the Rayleigh Plesset bubble growth equation [29, 30]:

$$\frac{p_v(T) - p}{\rho_l} = R\frac{d^2R}{dt} + 3/2(\frac{dR}{dt})^2 + -\frac{2\sigma}{\rho_l R} \tag{7}$$

Where p is local far-field pressure, p_v is the liquid-vapour pressure. R refers to the radius

of the bubble. ρ_l is the liquid density, and σ refers to the surface tension of the liquid.

The vapour Transport Equation derived from Schnerr and Sauer is given as follows:

$$\frac{\partial(\rho_v \alpha_v)}{\partial t} + \nabla(\rho_v \alpha_v u_i) = \frac{\rho_v \rho_l}{\rho} \frac{d\alpha_v}{dt} \tag{8}$$

Where ρ_v and ρ_l represent the density of the vapour and liquid phase respectively. The relation between the vapour volume fraction α_v and the number of bubbles is expressed as follows:

$$\alpha_v = n\frac{4}{3}\pi R^3/(1 + n\frac{4}{3}\pi R^3) \tag{9}$$

The mass transfer rate $\dot{m}$ can be calculated with the Eq. (10)

$$\dot{m} = \frac{\rho_v \rho_l}{\rho} \alpha_v (1 - \alpha_v) \frac{3}{R} \frac{dR}{dt} = \begin{cases} \frac{\rho_v \rho_l}{\rho} \alpha_v (1 - \alpha_v) \frac{3}{R} \left(\frac{2(p_v - p)}{3\rho_l}\right)^{1/2} & (p \le p_v) \\ \frac{\rho_v \rho_l}{\rho} \alpha_v (1 - \alpha_v) \frac{3}{R} \left(\frac{2(p - p_v)}{3\rho_l}\right)^{1/2} & (p_v \le p) \end{cases} \tag{10}$$

The governing equations were discretised by implicit Euler schemes. The convection terms in momentum and continuity equations were discretised by the second-order central difference schemes, while other equations were discretised by the first-order upwind difference scheme. The diffusion term was discretised by Gauss linear scheme. In order to avoid divergence, the Gauss van Leer difference scheme was used for the convection term of Eq. (9) because of a phase step between the gas and liquid [31]. Moreover, the Pressure Implicit with Split Operator (PISO) algorithm suited to transient calculation was utilized to couple the solutions of mass and momentum equations [32].

Fig. 4 illustrates the computational domain mesh. The length and diameter of the injector orifice were 2 mm and 0.3 mm respectively. The diameter of the upper end of circular table shaped chamber is 0.6 mm, while the diameter of the upper end is 0.8 mm. The length of the

chamber was 5 mm. The initial numerical parameters (e.g. fuel properties, pressures and temperatures) were consistent with the experiment. The total number of grids was 1337,851, and the minimum cell size was 0.026 mm. In order to accurately simulate the practical fuel injection process, 80% volume of the nozzle was filled with diesel fuel while the rest volume of the nozzle was filled with air at the beginning of the simulation [33].

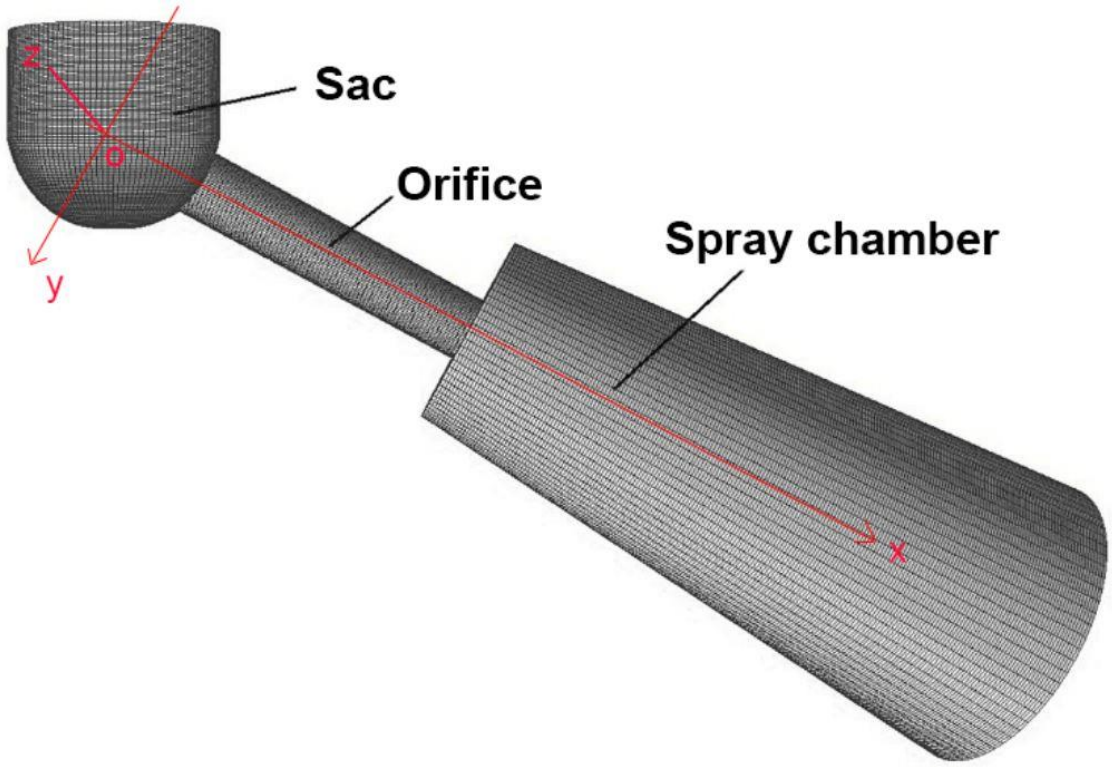

Fig. 4 The computational domain mesh

3. Results and discussion

3.1 The variations of the mass flow rate and jet velocity at the nozzle exit

Fig. 5a depicts the temporal variation of the fuel mass flow rate $\dot{m}$ under different injection pressures. It was found that the fuel mass flow rate increased with the increase of the injection pressure. The mass flow rate is very important for determining the heat release rate, cylinder temperature and emissions [34]. The fuel velocity in the outlet of orifice u was

calculated by the following equation:

$$u = 4\dot{m}/\rho_l \pi d^2 \tag{11}$$

Where ρ_l and d are the density of test fuel and the diameter of the nozzle orifice. The variations of the jet velocity in the outlet of the nozzle were demonstrated in Fig. 5b. The jet velocity had similar variation trends with the mass flow rate.

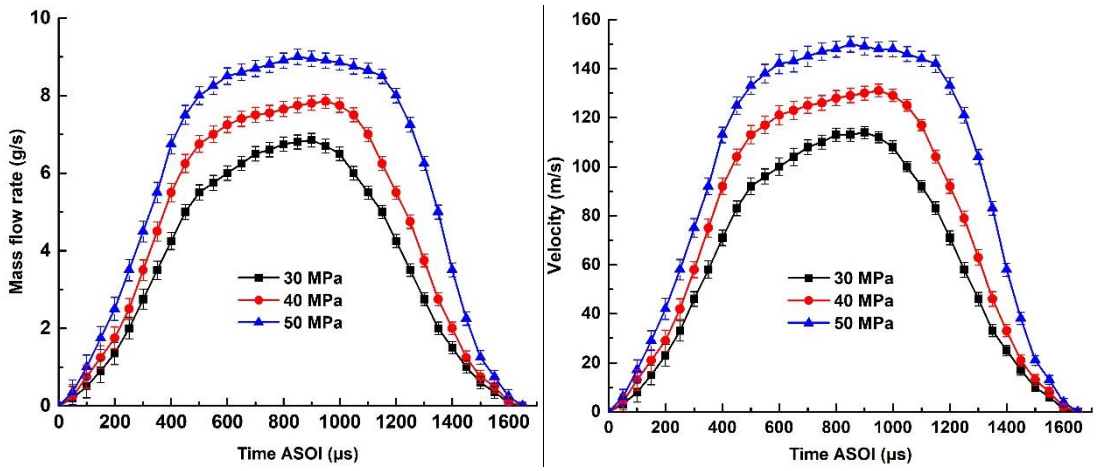

Fig. 5 The temporal variations of the fuel mass flow rate and jet velocity at the nozzle exit

3.2 Typical morphologies of the penetrating jet

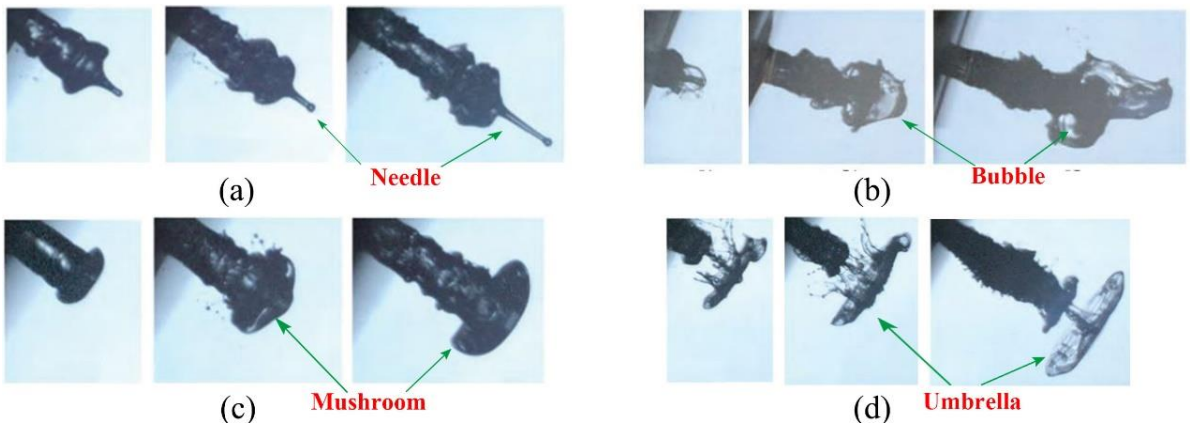

Fig. 6 The typical morphologies of the diesel jet

Fig. 6 illustrates that there were four types of morphology of the diesel jet in the experimental images: (a) a tiny liquid column propelled from the mainstream; (b) a bubble existed in the

tip of liquid jet, which was probably formed by the reverse flow of ambient gas into nozzle; (c) a mushroom-like tip constructed in the front of the liquid jet along the axial direction; (d) an umbrella-shaped head with a neck formed in the liquid jet tip. The statistical data from the obtained images showed that the first type mentioned above was more likely to occur at low injection pressure.

The initial breakup process of the diesel jet under the injection pressure of 30 MPa was presented in Fig. 7. It was found that a liquid column with the diameter of 54 μm appeared in front of the diesel jet at the very beginning of the injection, which indicated that the jet velocity in the central position of the jet tip was larger than that in the edge position. The similar appearance was reported in the literature [19], and the reason for this phenomenon was attributed to the existence of the nozzle-trapped fluid generated by the former injection event. Detailed analysis of the tiny liquid column was also conducted by using numerical simulation, which will be discussed later. At 50 μs, a mushroom head was observed in the front end of the liquid jet, which was almost consistent with the third type of the spray structure showed in Fig. 6c. The formation mechanism and growth of the ‘mushroom’ have been studied by previous researchers [16, 35] and the main reason for ‘mushroom’ formation was ascribed to the flow state inside the nozzle while the fuel radial expansion at the beginning was regarded as the primary cause for its growth.

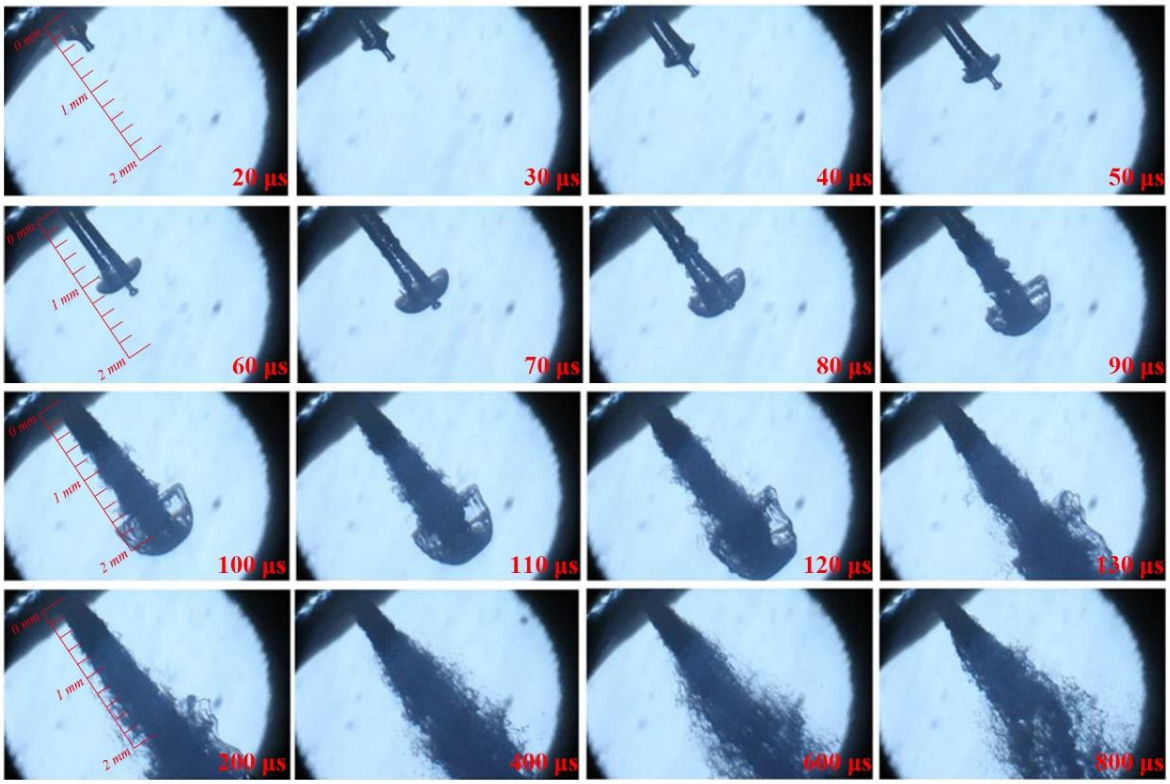

Fig. 7 The temporal evolution of diesel jet in the near-nozzle region under the injection pressure of 30 MPa at the atmospheric ambient

As injection went on, the ‘mushroom’ gradually enlarged in radial and axial directions. The radial expansion might originally result from the initial acceleration of the penetrating jet during the opening period of the needle valve [19], and the axial expansion could be explained by the increasing jet velocity in the outlet of the nozzle. Furthermore, the radial expansion indicated that the ‘mushroom’ was inflated by the upstream fluid and then stabilized by the fluid surface tension. At the time of 70 μs, the liquid column in the jet tip was caught up with the ‘mushroom’ as a result of the resistance force of the ambient air. At 90 μs, a few bubbles were observed inside the ‘mushroom’, which might originate from the vaporised fuel trapped inside the nozzle. The bubbles gave rise to the formation of the ligaments and droplets in the tip, which was favourable for the spray breakup as well as the

engine combustion and emissions.

The observation of Fig. 5 and Fig. 7 shows that the jet velocity at the nozzle exit had an influence on the surface instability of the liquid jet. During the injection time range of 0 to 70 μs, the outlet jet velocity and Reynold number were small (Fig. 5), thus the ambient air had a negligible effect on the jet surface, hence the jet surface was smooth in this period (Fig. 7). From 70 to 100 μs, the jet surface became unstable and ligaments occurred in the surface due to the increasing relative velocity between the jet and the surrounding gas. However, there was still not obvious stripping phenomenon of the ligaments in this period. After 100 μs, the turbulence inside the jet was intensified gradually due to the rising jet velocity, and thus the radial velocity component of the jet generated by the turbulence would spur the detachment of the liquid ligaments and droplets from the jet surface. Moreover, the interaction between the jet and ambient air was stronger than before, and the aerodynamic shear force was enhanced correspondingly, which would contribute to the formation of the ligaments and droplets.

3.3 Spray structure at different injection pressures

The influence of injection pressure on the initial structure of jet was illustrated in Fig. 8. It was observed that the increase of the injection pressure caused the earlier emergence of the surface instability as marked by red rectangles in Fig. 8a and Fig. 8b. For instance, the initial times of detecting the disturbance in the jet surface under 30 MPa and 40 MPa injection pressures were about 70 μs and 50 μs, and the surface disturbance at 50 MPa appeared before 40 μs.

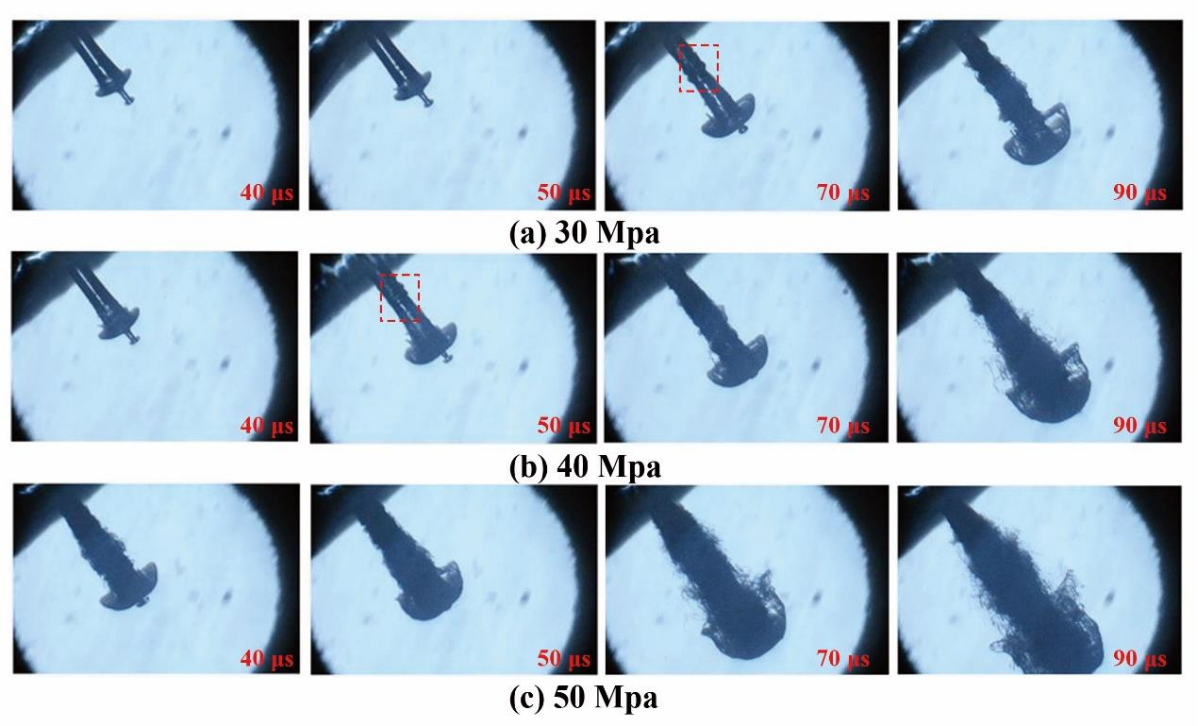

Fig. 8 The temporal evolution of diesel jet in near-field under the injection pressures of (a) 30 MPa, (b) 40 MPa and (c) 50 MPa at the atmospheric ambient

Fig. 9 presents the variations of the spray penetrations and angles at the three injection pressures. It can be observed that the higher injection pressure led to longer penetration. Because the kinematic energy of the injected fuel would greatly improve in the high pressures. Besides, the effect of the injection pressure increment on the spray penetration was small in the early stage of injection and gradually became large with the injection time (Fig. 9a). The spray angles at the two injection pressures 40 MPa and 50 MPa were apparently greater than that at the injection pressure of 30 MPa. However, the relationship between the spray angles at the two high pressures (40 MPa and 50 MPa) was not clear (Fig. 9b). The radial velocity component of the jet and the disordered movement of liquid ligaments and droplets were the primary factors that influenced the spray angles [13]. In addition, it is noteworthy that the spray penetration would increase by about 9% as increased each 10 MPa injection pressure.

The similar rule was not found for spray angle.

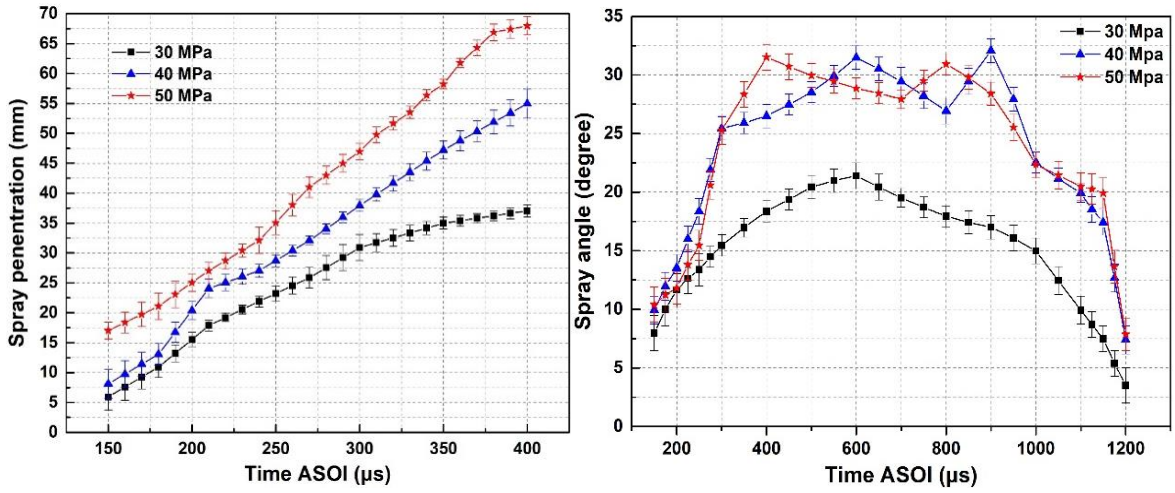

(a) (b)

Fig. 9 The temporal evolutions of (a) the spray angle and (b) the spray angle under different injection pressures (30, 40, 50 MPa) at the atmospheric ambient

3.4 Spray structure at different ambient pressures

The temporal evolutions of the diesel jet spray structure in the near-nozzle field under different ambient pressures were shown in Fig. 10. More liquid ligaments and droplets were observed in the higher ambient pressures compared with the lower ambient pressure cases. The reason behind this phenomenon was that the growing ambient pressure increased the density of the ambient air, thus the air drag force was strengthened to promote the breakup of the liquid jet. It is interesting to find that the small liquid column in the tip transformed into an umbrella-like structure under the ambient pressures of 0.5 MPa and 1 MPa as marked by red circles (Fig. 10). This transformation was attributed to the aerodynamic shear force squeezing the protruding liquid column and causing the liquid dispersion from the centre to the periphery. The development of the spray was strongly frustrated and the penetration length was shorter under the ambient pressure of 2 MPa (Fig. 10d).

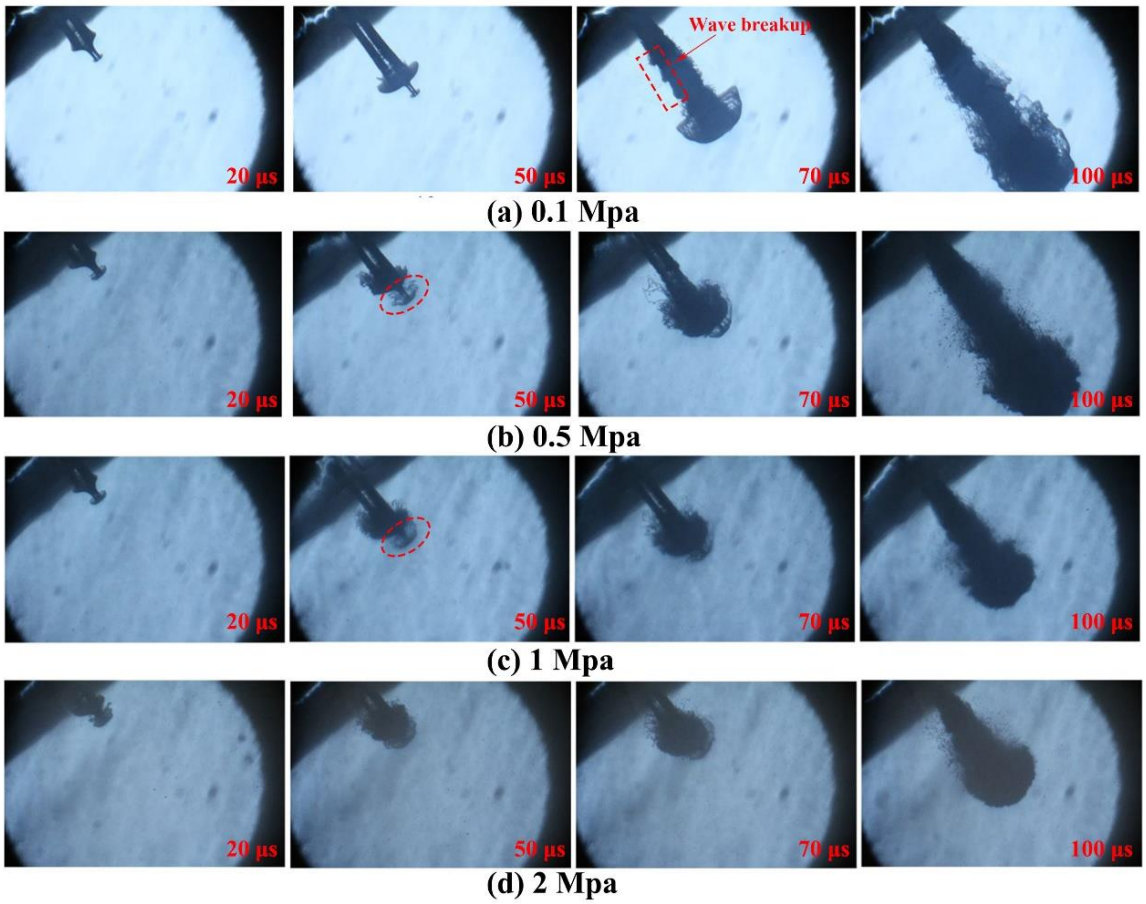

Fig. 10 The temporal evolution of diesel jet in the near-nozzle region under the ambient pressures of (a) 0.1 MPa, (b) 0.5 MPa, (c) 1.0 MPa and (d) 2.0 MPa at 40 MPa injection pressure

Results presented at Fig. 10 shown that the statistical mean size of the bigger observable liquid parcels at 100 μs decreased from larger than 80 μm to smaller than half the size as increased ambient pressure from 0.5 to 1.0 MPa. In addition, the surface wave was detected on the boundaries of the jet at the time of 70 μs in Fig. 9a and the magnified part of the figure were illustrated in Fig. 11. Further details about the development of the surface wave could be recognized from Fig. 11. Firstly, the wave amplitude increased from the outlet of the nozzle along with the axial direction. Then the wave began to split when the wave amplitude

was large enough. Similar phenomena were found in Ref. [36].

The amplitude and frequency of the wave appeared in Fig. 11 were determined in this work. The measured wavelength λ at the operating point was 120 μm, and the velocity u at the boundary was about 15 m/s which was calculated by using two adjacent images. The wave frequency $f = u/\lambda$ was calculated at 125 kHz. The amplitude height h was measured at about 25 μm before the breakup of the wave.

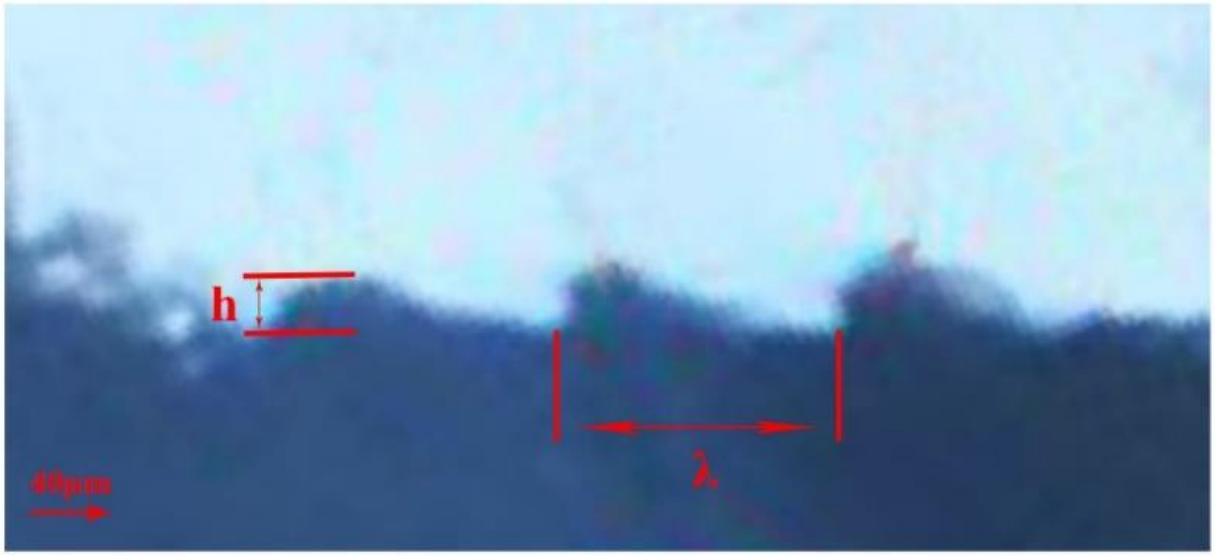

Fig. 11 The surface wave of the diesel jet under 30 MPa injection pressure and 0.1 MPa ambient pressure

The effects of different ambient pressures on the spray characteristics were presented in Fig. 12. It was commonly accepted that the penetration length decreased as increased the ambient pressure. Because the air density increased with the rise of the ambient pressure, which led to the number of air molecules impinging on the jet increasing, and the loss of the jet kinetic energy correspondingly increased, and thus the jet velocity decreased, the spray penetration decreased as well. The spray penetration roughly decreased about 10% with increasing each 0.5 MPa ambient pressure. Besides, the spray angle also increased with the escalation of the

ambient pressure. The overall variation trends of the spray angle under different ambient pressures were similar. And the relationships between the spray angle and the injection time were nearly linear before the time of 300 μs for all the cases.

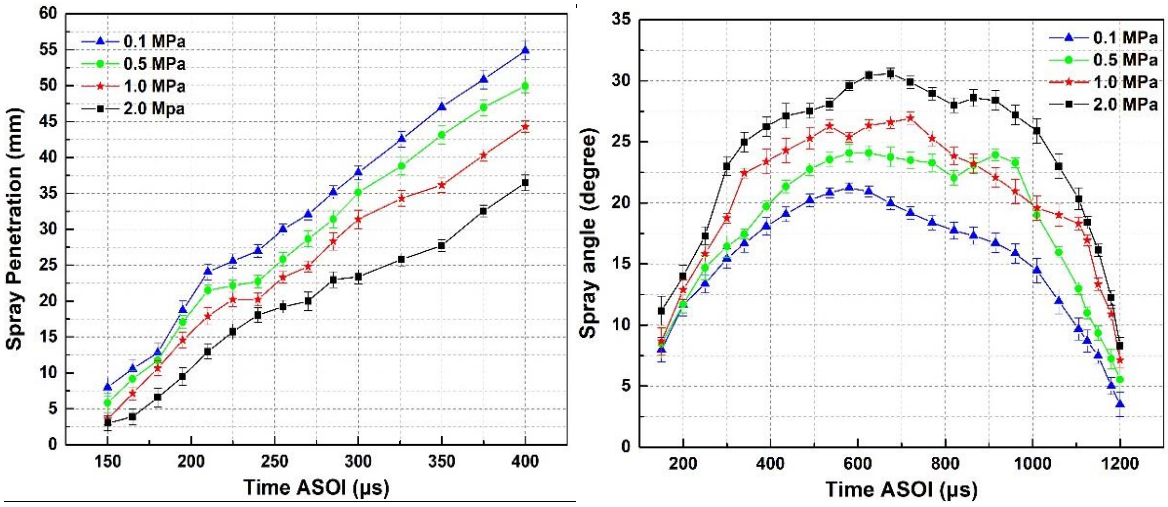

(a) (b)

Fig. 12 The temporal evolutions of (a) the spray angle and (b) the spray angle under the ambient pressure of 0.1, 0.5, 1 and 2 MPa at 30 MPa injection pressure

3.5 The numerical analysis for liquid column formation in the jet tip

For the numerical simulation, a bubble with a diameter of 0.1 mm was placed inside the nozzle as shown in Fig. 13a and the bubble was surrounded by the residual fluid. At the time of 5 μs, the initial bubble was compressed by the upstream fuel propelling the downstream fuel to the nozzle exit. It was found that the bubble was split into two sections by the upstream fuel at 7.5 μs because the jet velocity in the central line was higher than that at the periphery. At the time of 20 μs, the initial spray structure featured a small liquid column in the tip. The mushroom-shaped head gradually appeared after 20 μs, and some liquid droplets were observed in the surrounding of the liquid column. The liquid column was found to become thinner and more unstable at the time of 50 μs.

The simulation results in the cases without the initial bubble inside the nozzle were presented in Fig. 13a. Although the overall variation trend of the jet injection was similar with that in the case with the initial bubble, there was no liquid column propelled from the jet tip, which proved that the liquid column appeared in the tip of the liquid jet was due to the existence of the initial bubble inside the nozzle.

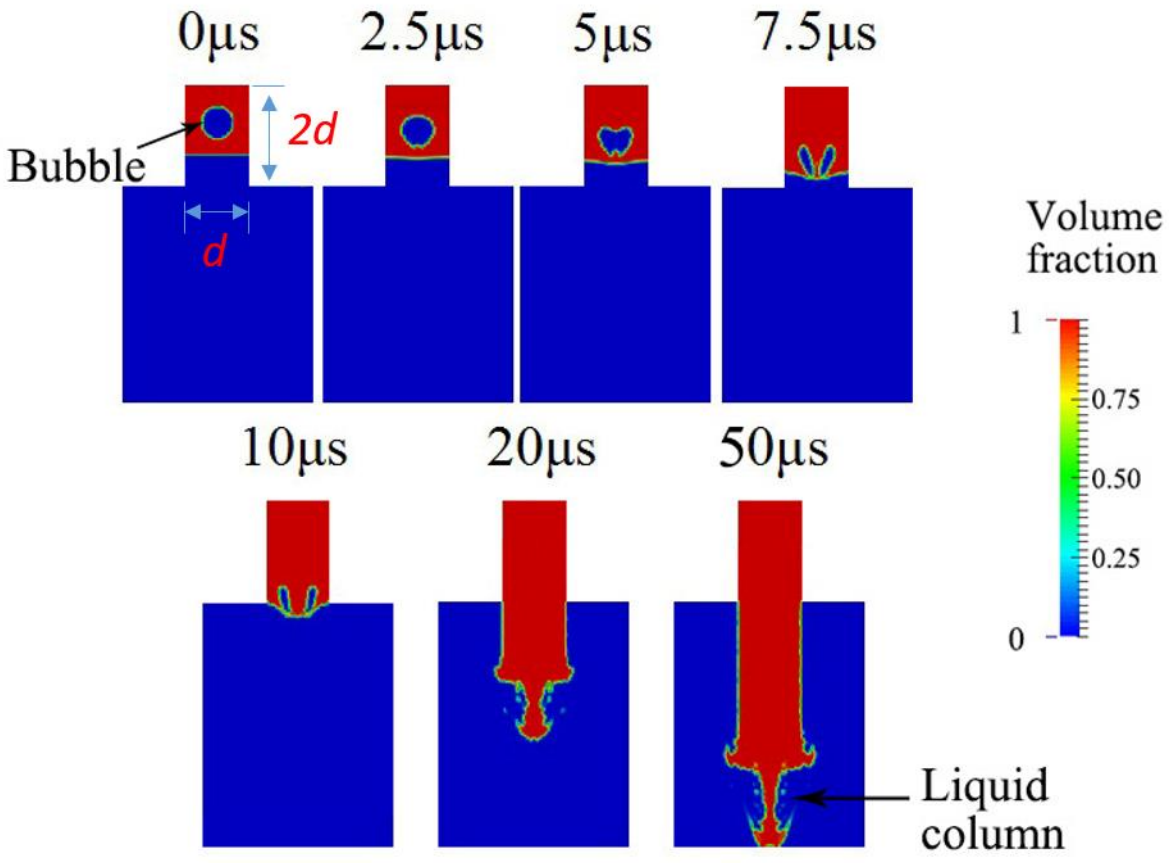

(a) With the initial bubble

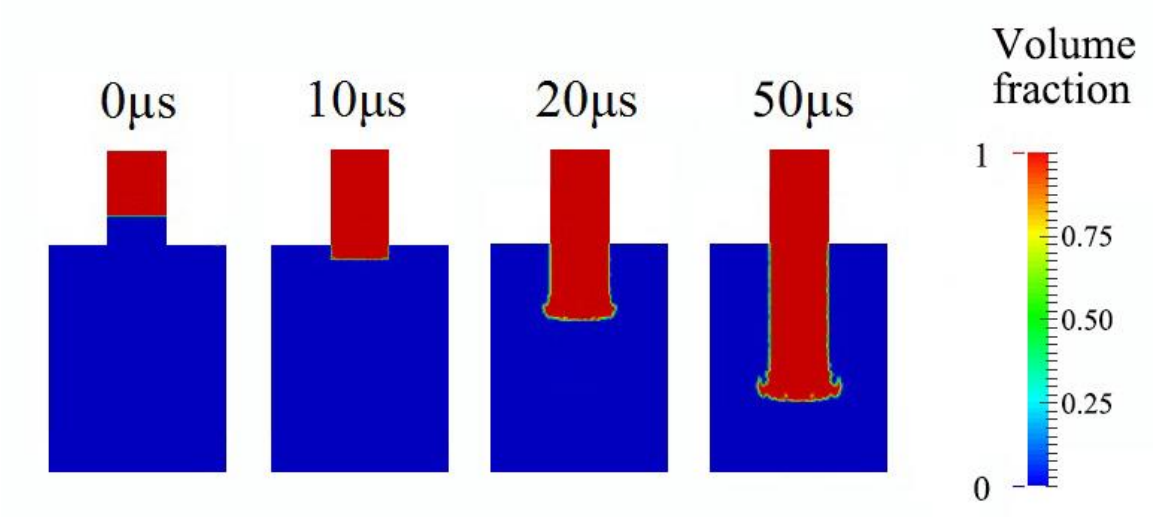

(b) Without the initial bubble

Fig. 13 Simulation results of the diesel jet injection (a) with the initial bubble and (b) without the initial bubble inside the nozzle

The comparison results between the experiment and the simulation with the initial bubble at different ambient pressures (0.1 MPa and 1.0 MPa) were illustrated in Fig. 14. The mushroom head morphology and the liquid column in the tip were significantly affected by the increasing ambient pressure, and correspondingly there were more droplets appeared in the simulation. The liquid ligaments stripping from the edges of the mushroom were accurately observed both in the experimental images and the simulation results. In addition, it can be seen from Fig. 14 that the simulated results exhibited a favourable agreement with the experimental results. However, there were still some deviations between the numerical and experimental results, since the initial bubble in the simulation could not completely reproduce the initial bubble in the experiment in terms of its size and in-nozzle position.

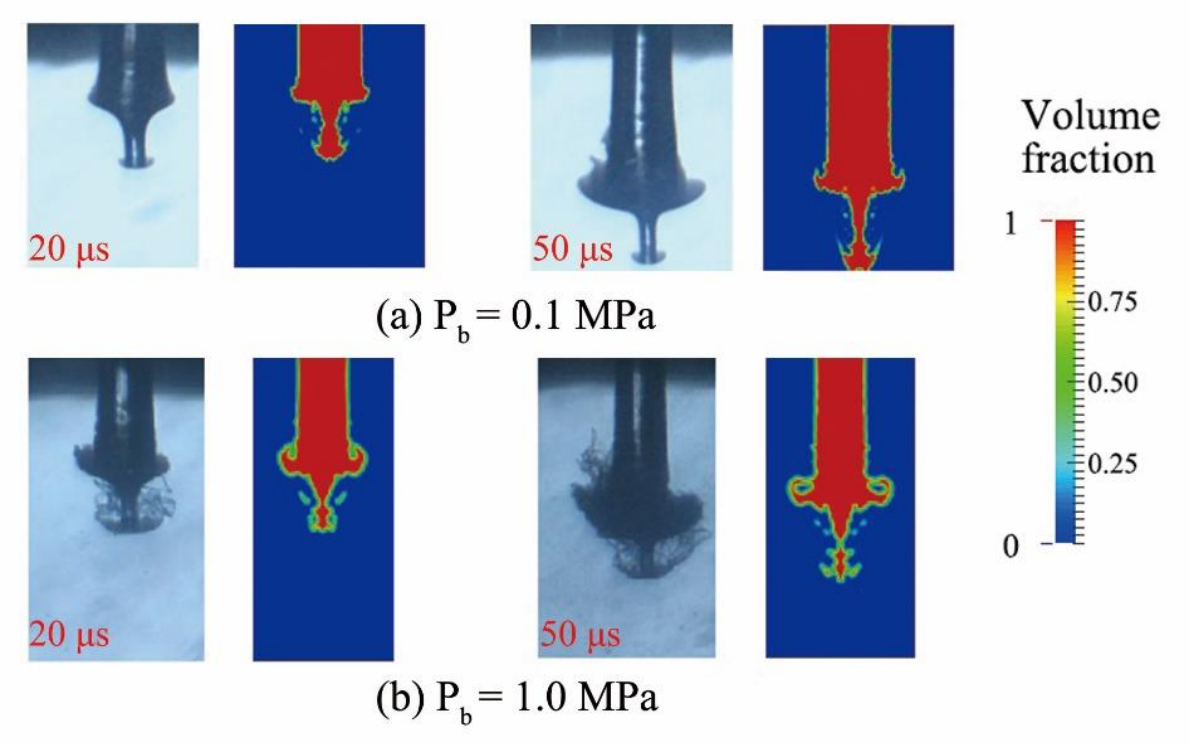

Fig. 14 Comparison between numerical results and experimental data under the ambient pressure of (a) 0.1 MPa and (b) 1.0 MPa at 40 MPa injection pressure

4. Conclusions

In this paper, the evolution of the spray morphology in the near-nozzle field was experimentally investigated by using long-distance microscopic imaging technique. The formation mechanism of the liquid column in the tip of the liquid jet was numerically simulated based on LES theory and VOF interface capturing method for the first time. Main conclusions can be drawn as follows:

1. The variation of the injection pressure had a notable influence on the jet velocity and flow regime in the nozzle exit, which determined the evolution of the initial spray morphology of the fuel jet.

2. The initial spray morphology was remarkably affected by the injection pressure and ambient pressure. Besides, the ambient pressure exhibited a significant impact on the

maximum size of the observable droplets.

3. The spray penetration decreased by approximately 10% with the increment of 0.5 MPa in ambient pressure, while increased by about 9% with 10 MPa injection pressure increment. There was no definite quantitative relationship between spray angle and injection parameters.

4. A small liquid column was observed in the spray tip, and the corresponding numerical study revealed that it originated from residual bubbles trapped inside the nozzle.

Acknowledgements

This research is supported by National Natural Science Foundation of China (91641119) and the sponsorship from China Scholar Council (201806020055). The authors also would like to thank the support from Cao Guang Biao High Tech Talent Fund, Zhejiang University.

Reference

[1] Hoang AT. Experimental study on spray and emission characteristics of a diesel engine fueled with preheated bio-oils and diesel fuel. Energy. 2019;171:795-808.

[2] Su HP, Kim HJ, Chang SL. Numerical Investigation of Combustion and Exhaust Emissions Characteristics Based on Experimental Spray and Atomization Characteristics in a Compression Ignition Diesel Engine. Energy & Fuels. 2010;24(4):780-7.

[3] Lee S, Lee CS, Park S, Gupta JG, Maurya RK, Agarwal AK. Spray characteristics, engine performance and emissions analysis for Karanja biodiesel and its blends. Energy. 2017;119:138-51.

[4] Alkhedhair A, Guan Z, Jahn I, Gurgenci H, He S. Water spray for pre-cooling of inlet air for Natural Draft Dry Cooling Towers – Experimental study. International Journal of Thermal Sciences. 2015;90:70-8.

[5] Soid SN, Zainal ZA. Spray and combustion characterization for internal combustion engines using optical measuring techniques – A review. Energy. 2011;36(2):724-41.

[6] Park SH, Lee CS. Combustion performance and emission reduction characteristics of automotive DME engine system. Progress in Energy & Combustion Science.

2013;39(1):147-68.

[7] Hyunkyu S, Changsik L. A review on atomization and exhaust emissions of a biodiesel-fueled compression ignition engine. Renewable & Sustainable Energy Reviews. 2016;58:1601-20.

[8] Sun Y, Alkhedhair AM, Guan Z, Hooman K. Numerical and experimental study on the spray characteristics of full-cone pressure swirl atomizers. Energy. 2018;160:678-92.

[9] Roisman IV, Araneo L, Tropea C. Effect of ambient pressure on penetration of a diesel spray. International Journal of Multiphase Flow. 2007;33(8):904-20.

[10] He C, Ge Y, Tan J, Han X. Spray properties of alternative fuels: A comparative analysis of biodiesel and diesel2008.

[11] Li Y, Xu H. Experimental study of temporal evolution of initial stage diesel spray under varied conditions. Fuel. 2016;171:44-53.

[12] Manin J, Bardi M, Pickett LM, Dahms RN, Oefelein JC. Microscopic investigation of the atomization and mixing processes of diesel sprays injected into high pressure and temperature environments. Fuel. 2014;134(9):531-43.

[13] Wei M, Gao Y, Yan F, Chen L, Feng L, Li G, et al. Experimental study of cavitation formation and primary breakup for a biodiesel surrogate fuel (methyl butanoate) using transparent nozzle. Fuel. 2017;203:690-9.

[14] Gao Y, Wei M, Yan F, Chen L, Li G, Feng L. Effects of cavitation flow and stagnant bubbles on the initial temporal evolution of diesel spray. Experimental Thermal and Fluid Science. 2017;87:69-79.

[15] Hattori H, Narumiya K, Tsue M, Kadota T. Analysis of initial breakup mechanism of diesel spray injected into high-pressure ambience. SAE Technical Paper; 2004.

[16] Wang Z, Ding H, Ma X, Xu H, Wyszynski ML. Ultra-high speed imaging study of the diesel spray close to the injector tip at the initial opening stage with single injection. Applied Energy. 2016;163:105-17.

[17] Fu W, Li F, Meng K, Liu Y, Shi W, Lin Q. Experiment and analysis of spray characteristics of biodiesel blending with di-n-butyl ether in a direct injection combustion chamber. Energy. 2019.

[18] Ding H, Wang Z, Li Y, Xu H, Zuo C. Initial dynamic development of fuel spray analyzed by

ultra high speed imaging. Fuel. 2016;169:99-110.

[19] Crua C, Heikal MR, Gold MR. Microscopic imaging of the initial stage of diesel spray formation. Fuel. 2015;157:140-50.

[20] Desantes JM, Payri R, Salvador FJ, Morena JDL. Influence of cavitation phenomenon on primary break-up and spray behavior at stationary conditions. Fuel. 2010;89(10):3033-41.

[21] Shinjo J, Umemura A. Simulation of liquid jet primary breakup: Dynamics of ligament and droplet formation. International Journal of Multiphase Flow. 2010;36(7):513-32.

[22] Ghiji M, Goldsworthy L, Brandner PA, Garaniya V, Hield P. Numerical and experimental investigation of early stage diesel sprays. Fuel. 2016;175(1):274-86.

[23] Xiao F, Dianat M, Mcguirk JJ. LES of turbulent liquid jet primary breakup in turbulent coaxial air flow. International Journal of Multiphase Flow. 2014;60(2):103-18.

[24] Battistoni M, Xue Q, Som S. Large-Eddy Simulation (LES) of Spray Transients: Start and End of Injection Phenomena. Oil Gas Sci Technol – Rev IFP Energies nouvelles. 2016;71(1):4.

[25] Yuan W, Sauer J, Schnerr GH. Modeling and computation of unsteady cavitation flows in injection nozzles. Mécanique & Industries. 2001;2(5):383-94.

[26] Payri R, Tormos B, Gimeno J, Bracho G. Large Eddy Simulation for high pressure flows: Model extension for compressible liquids. Mathematical and Computer Modelling. 2011;54(7):1725-31.

[27] Piomelli U. Large-eddy simulation: achievements and challenges. Progress in Aerospace Sciences. 1999;35(4):335-62.

[28] Sone K, Patel N, Menon S. Large-eddy simulation of fuel-air mixing in an internal combustion engine. Aiaa Journal. 2013.

[29] Rayleigh L. VIII. On the pressure developed in a liquid during the collapse of a spherical cavity. The London, Edinburgh, and Dublin Philosophical Magazine and Journal of Science. 1917;34(200):94-8.

[30] Plesset MS. The dynamics of cavitation bubbles. Journal of applied mechanics. 1949;16:277-82.

[31] Jasak H. Error analysis and estimation for the finite volume method with applications to fluid flows. 1996.

[32] Issa RI. Solution of the implicitly discretised fluid flow equations by operator-splitting.

Journal of Computational Physics. 1986;62(1):40-65.

[33] Ghiji M, Goldsworthy L, Brandner PA, Garaniya V, Hield P. Analysis of diesel spray dynamics using a compressible Eulerian/VOF/LES model and microscopic shadowgraphy. Fuel. 2017;188:352-66.

[34] Wang Z, Wyszynski ML, Xu H, Abdullah NR, Piaszyk J. Fuel injection and combustion study by the combination of mass flow rate and heat release rate with single and multiple injection strategies. Fuel Processing Technology. 2015;132:118-32.

[35] Badock C, Wirth R, Fath A, Leipertz A. Investigation of cavitation in real size diesel injection nozzles. Intjheat Fluid Flow. 1999;20(5):538-44.

[36] Heimgärtner C, Leipertz A. Investigation of the Primary Spray Breakup Close to the Nozzle of a Common - Rail High Pressure Diesel Injection System. SAE International; 2000.